ANNUAL REVIEWS

Annual Review of Physical Chemistry

Chiral Plasmonic Nanostructures Enabled by Bottom-Up Approaches

Maximilian J. Urban,[1,2,*] Chenqi Shen,[3,4,*] Xiang-Tian Kong,[5,*] Chenggan Zhu,[3] Alexander O. Govorov,[5,6] Qiangbin Wang,[3,4] Mario Hentschel,[7] and Na Liu[1,2]

[1]Max Planck Institute for Intelligent Systems, 70569 Stuttgart, Germany; email: na.liu@kip.uni-heidelberg.de

[2]Kirchhoff-Institute for Physics, University of Heidelberg, 69120 Heidelberg, Germany

[3]CAS Key Laboratory of Nano-Bio Interface, Division of Nanobiomedicine Research, and *i*-Lab, Suzhou Institute of Nano-Tech and Nano-Bionics, Chinese Academy of Sciences, Suzhou 215213, China; email: qbwang2008@sinano.ac.cn

[4]College of Materials Science and Opto-Electronic Technology, University of Chinese Academy of Sciences, Beijing 100049, China

[5]Department of Physics and Astronomy, Ohio University, Athens, Ohio 45701, USA; email: govorov@ohio.edu

[6]Institute of Fundamental and Frontier Sciences, University of Electronic Science and Technology of China, Chengdu 610054, China

[7]4th Physics Institute and Stuttgart Research Center of Photonic Engineering (SCoPE), University of Stuttgart, 70569 Stuttgart, Germany; email: m.hentschel@physik.uni-stuttgart.de

Annu. Rev. Phys. Chem. 2019. 70:275–99

First published as a Review in Advance on May 21, 2019

The *Annual Review of Physical Chemistry* is online at physchem.annualreviews.org

https://doi.org/10.1146/annurev-physchem-050317-021332

*These authors contributed equally to this article

Keywords

plasmonics, chirality, nanostructures, circular dichroism, chiroptical responses, optical activity

Abstract

We present a comprehensive review of recent developments in the field of chiral plasmonics. Significant advances have been made recently in understanding the working principles of chiral plasmonic structures. With advances in micro- and nanofabrication techniques, a variety of chiral plasmonic nanostructures have been experimentally realized; these tailored chiroptical properties vastly outperform those of their molecular counterparts. We focus on chiral plasmonic nanostructures created using bottom-up approaches, which not only allow for rational design and fabrication but most

intriguingly in many cases also enable dynamic manipulation and tuning of chiroptical responses. We first discuss plasmon-induced chirality, resulting from the interaction of chiral molecules with plasmonic excitations. Subsequently, we discuss intrinsically chiral colloids, which give rise to optical chirality owing to their chiral shapes. Finally, we discuss plasmonic chirality, achieved by arranging achiral plasmonic particles into handed configurations on static or active templates. Chiral plasmonic nanostructures are very promising candidates for real-life applications owing to their significantly larger optical chirality than natural molecules. In addition, chiral plasmonic nanostructures offer engineerable and dynamic chiroptical responses, which are formidable to achieve in molecular systems. We thus anticipate that the field of chiral plasmonics will attract further widespread attention in applications ranging from enantioselective analysis to chiral sensing, structural determination, and in situ ultrasensitive detection of multiple disease biomarkers, as well as optical monitoring of transmembrane transport and intracellular metabolism.

1. INTRODUCTION

Humans are eager to understand the properties of matter and also strives to manipulate matter at will. For centuries, alchemists and scientists have endeavored to control and tailor the properties of matter. Many sophisticated techniques have been invented over time, including deposition, etching, doping, synthesis, and self-assembly. One of the most striking material properties of matter is visual appearance, that is, its reflectivity, absorptivity, and most importantly its color. Among the earliest examples of tailored visual appearances is colored glass. Some colored glass was later discovered to contain nano-sized gold (Au) particles. Such glass, coined cranberry glass, represents one of the earliest human-made nanostructured materials—obviously unknown at the time.

The origin of the colors lies in the absorption and scattering behavior of the metal nanoparticles in glass (1). When light impinges on a metal particle of a few tens of nanometers in diameter, collective oscillations of the quasi-free conduction electrons are excited with respect to the ionic background. One terms this resonant excitation a plasmon or, more accurately, a plasmon polariton (2). What makes plasmons so special? On one hand, the metal particles can be good scatterers and absorbers when interacting with light. On the other hand, the plasmonic resonance position, that is, the position of the most efficient scattering or absorption, can be tuned via the size, material, and surroundings of the particle (3). Thus, metal nanoparticles can be manipulated to exhibit bright and vivid colors, given their plasmonic resonances are in the visible wavelength range.

What makes plasmonic resonances more interesting is their ability to interact with each other. The harmonic oscillations of the conduction electrons give rise to plasmonic near-fields, regions of strong localized electromagnetic fields within subwavelength volumes (4, 5). When the local fields of adjacent nanoparticles overlap, coupling among the particles is mediated. In direct analogy to molecular hybridization and the formation of shared orbitals, the plasmonic resonances of adjacent particles can mix and hybridize, giving rise to collective resonant modes spanning the entire structure (6). The extraordinary number of possible coupling scenarios offers myriad schemes to design plasmonic nanostructures with tailored optical properties (7).

In the last decades, advances in micro- and nanotechnologies have enabled unprecedented opportunities to create complex plasmonic nanostructures according to a designer's wish. Top-down techniques, such as electron-beam lithography (8), focused ion beam etching (9), and direct laser writing (10), excel in realization of structural arrays and layered interfaces, whereas bottom-up

techniques, such as self-assembly and chemical synthesis (11), allow for more arbitrary structural geometries and richer possibilities of biochemical functionalization. A plethora of complex plasmonic architectures that draw direct analogies to natural molecules have been designed and investigated over the years. As a matter of fact, one may argue that significant research on plasmonic nanostructures has taken inspiration from natural molecules, given their beautiful physics and chemistry (12).

One of the most fascinating molecular motifs is chirality. A chiral or handed structure cannot be superimposed with its mirror image. Every chiral object therefore may exist in two distinct handednesses, called enantiomorphs or enantiomers. Chiral objects are ubiquitous in nature, ranging from macroscopic systems such as seashells to molecular systems such as carbohydrates. Interestingly, many chiral biomolecules are found only in one handedness. For instance, all essential amino acids are L-enantiomers, meaning D-enantiomers are absent. This phenomenon, called homochirality, has long intrigued researchers. However, a conclusive interpretation remains elusive (13).

Apart from the structural aspect, chirality can also manifest itself optically. A chiral structure that is optically active can absorb left- and right-handed circularly polarized light (LCP and RCP, respectively) differently. This phenomenon is called circular dichroism (CD) (14). Moreover, a chiral structure can also cause the rotation of linearly polarized light, called optical rotatory dispersion (ORD), resulting from different refractive indices for LCP and RCP light when interacting with the chiral structure. CD and ORD are therefore Kramers–Kronig related (15).

Chirality is a structural property closely correlated with the spatial arrangement of the individual constituents in three dimensions. The optical responses of chiral structures are thus widely investigated in structure-related research. For instance, CD spectroscopy can be used to reliably report the handedness and even subtle conformational changes of chiral molecules. CD spectroscopy is thus a standard tool in biology and life sciences for chiral discrimination. One major hurdle, however, lies in the weak chiroptical responses of natural molecules. For most chiral molecules, their CD bands are located in the ultraviolet (UV) spectral region, and the asymmetry factor, which characterizes the strength of optical chirality, is very small. Even concentrated solutions give rise to polarization rotation of light by only a few millidegrees, rendering sensitive detection and analysis of chiral molecules with low amounts very difficult to achieve (16).

The aforementioned findings and challenges have motivated scientists to enhance the strength of molecular chirality, as well as to achieve pronounced and tunable chiroptical responses for different spectral regions using artificial plasmonic structures (17, 18). Some studies transfer the intriguing concept of molecular chirality directly to the realm of plasmonics, whereas others indeed combine the two fields altogether. Plasmonic structures can exhibit large chiroptical responses, orders of magnitude stronger than those of chiral molecules. These experiments have stimulated further research on understanding the interactions between plasmonic structures and chiral molecules, with the hope of enhancing and possibly spectrally manipulating optical chirality, rendering the detection of a few chiral molecules possible (19–21).

We present a comprehensive review of recent advances and developments in the field of chiral nanoplasmonics. We focus on chiral plasmonic nanostructures created via synthesis methodologies, following an outline of (*a*) plasmon-induced chirality, chiral molecules in the vicinity of achiral plasmonic nanoparticles; (*b*) intrinsically chiral colloids, plasmonic particles that are chiral objects themselves; and (*c*) plasmonic chirality, achiral plasmonic particles arranged into handed configurations on static and active templates. Finally, we elucidate possible future directions and perspectives on the remaining challenges and open opportunities in this field.

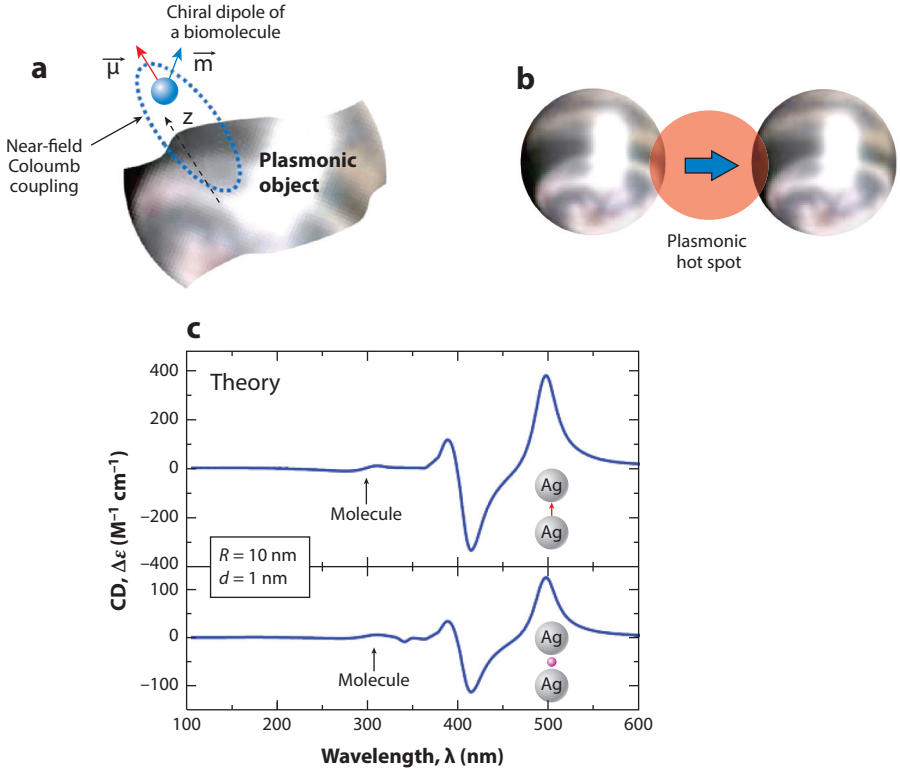

Figure 1

Theory of plasmon-induced chirality. (*a*) Schematic of a hybrid system containing a chiral molecule in the vicinity of a plasmonic object. (*b*) Schematic of an Ag dimer with a chiral molecule in the gap region. (*c*) Calculated circular dichroism (CD) spectrum for the electric dipole of the molecule parallel to the dimer axis; calculated CD spectrum averaged over the molecular orientations. Panel *a* adapted with permission from Reference 43; panels *b* and *c* adapted with permission from Reference 151.

2. PLASMON-INDUCED CHIRALITY

2.1. Theoretical Background

CD signals from natural chiral molecules are typically very weak and occur in the UV spectral range (150–300 nm) (22). Considerable effort has been devoted to enhancing the CD signals of chiral molecules, as well as to bringing chiroptical responses to the visible and near-infrared regions. The local near-fields generated by a metal nanoparticle upon light illumination can mediate the interaction of the particle and a chiral molecule placed in close proximity. In this case, a new CD line is induced and occurs near the plasmonic resonance position of the metal nanoparticle. This is termed plasmon-induced chirality (23–31).

Theoretically, the CD responses of a hybrid system containing a chiral molecule and a metal nanoparticle (see **Figure 1*a***) can be written as (32)

$$\mathrm{CD}_{\mathrm{total}} = \mathrm{CD}_{\mathrm{molecule}} + \mathrm{CD}_{\mathrm{plasmon\text{-}induced}}, \qquad 1.$$

where $\mathrm{CD}_{\mathrm{molecule}}$ and $\mathrm{CD}_{\mathrm{plasmon\text{-}induced}}$ are the CD signals from the differential dissipations of LCP and RCP light inside the molecule and the metal nanoparticle, respectively. The molecular CD

modified by the plasmonic near-fields can be written as (32, 33)

$$\mathrm{CD}_{\mathrm{molecule}} = E_0^2 \frac{8}{3}\sqrt{\varepsilon_0\omega_0}\frac{\Gamma}{|\hbar\omega - \hbar\omega_0 + i\Gamma|^2}\mathrm{Im}\left[\hat{P}\boldsymbol{\mu}_{12}\cdot\mathbf{m}_{21}\right]. \quad 2.$$

Here, we use SI units. E_0 and ε_0 are the incident electric field and matrix permittivity, respectively. The molecule is described by its electric and magnetic transition dipole moments, denoted using $\boldsymbol{\mu}_{12}$ and $\mathbf{m}_{21}$, respectively. The initial absorption line shape of the molecule is described by the energy, $\hbar\omega_0$, and broadening Γ of the molecular transition. The operator $\hat{P}$ is the matrix of the near-field enhancement at the position of the chiral molecule. The plasmonic near-field enhancement decreases as the distance between the molecule and metal surface increases. In the dipolar limit of the molecule–plasmon interaction, the plasmonic enhancement matrix is proportional to a^3/d^3, where a and d are the nanoparticle size and the separation between the molecule and the metal surface, respectively (32).

The second term in Equation 1 strongly depends on the shape and size of the metal nanoparticle. It can be explicitly expressed only for simple cases, such as for small spherical nanoparticles with dipolar approximations. In general, this term can be written as (32)

$$\mathrm{CD}_{\mathrm{plasmon\text{-}induced}} \propto \mathrm{Im}(\varepsilon_{\mathrm{metal}})\cdot f_{\mathrm{resonant}}\cdot\mathrm{Im}(\hat{K}\boldsymbol{\mu}_{12}\cdot\mathbf{m}_{21}). \quad 3.$$

Here $\varepsilon_{\mathrm{metal}}$ is the dielectric function of the metal. The operator $\hat{K}$ describes the interactions between the molecule and the plasmonic near-fields. The resonant factor, f_{resonant}, which strongly depends on the size and shape of the nanoparticle, describes the plasmonic enhancement in the metal.

Importantly, the hot spot generated between two metal nanoparticles can be exploited to amplify the plasmonic near-field enhancement (**Figure 1*b***). **Figure 1*c*** shows an example of the plasmon-induced CD from a silver (Ag) dimer. Both the molecular CD lines and the plasmon-induced CD lines are excited. Specifically, compared with the molecular CD, the plasmon-induced CD responses shift to longer wavelengths and are much stronger. It should be noted that the orientation of the electric dipole of the molecule considerably influences the amplitude of the plasmon-induced CD in an anisotropic system. In this case, the strongest plasmon-induced CD occurs, when the molecule dipole $\boldsymbol{\mu}_{12}$ is perpendicular to the metal surface. The plasmon-induced CD drops to approximately one-quarter of the strongest value when averaged over the dipole orientations, as shown in **Figure 1*c***.

The near-field theory of the plasmon-induced CD can be applied to cases in which the metal particles are much smaller compared with the operating wavelength of light, so that retardation effects are negligible (i.e., the spatial changes of the light phase within the nanoparticles are very small). However, the retardation should be included as a perturbation (34). It is noteworthy that the near-field effects alone are not sufficient to produce nonzero CD signals for randomly oriented complexes in a solution, because the CD effect involves a magnetic dipole moment of a chiral object (a molecule or a nanocrystal). Therefore, the CD effect requires the inclusion of the magnetic field of light (22). Strong retardation effects appear in large metal structures, which are comparable to or larger than the wavelength of light. In this case, the CD responses must be calculated by solving the full Maxwell's equations (34, 36). For a chiral medium, the constitutive relations can be written as (34, 36)

$$\begin{aligned}\mathbf{D} &= \varepsilon\mathbf{E} + i\xi_c\mathbf{B},\\ \mathbf{H} &= \frac{\mathbf{B}}{\mu} + i\xi_c\mathbf{E},\end{aligned} \quad 4.$$

where $\varepsilon = \varepsilon(\omega, \mathbf{r})$ is the permittivity, $\xi_c(\omega, \mathbf{r})$ describes the chiral property of the medium, and μ is the permeability. For nonmagnetic materials, such as Au, Ag, and chiral molecules, $\mu = 1$. In general, one can identify two major mechanisms in hybrid nanostructures incorporating metal particles and chiral media: the strong near-field plasmon-induced CD and the far-field electromagnetic CD (34, 36). The first mechanism depends critically on the anisotropy of a plasmon–molecular complex; for example, for spherically symmetric structures, it can be weak. The second mechanism gives rise to strong CD signals in large nanostructures in which the retardation effects govern the optical responses and the light–matter interaction. This mechanism can be calculated analytically (34, 36).

2.2. Experimental Realizations

Attaching chiral ligands on the surfaces of achiral metal nanoparticles is an efficient and convenient route to chemically acquiring optical chirality in the visible spectral range (32, 33, 37–41). To achieve strong CD from such complexes, metal particles with different morphologies, including nanorods (NRs) (42) and nanocubes (43), have been employed owing to their pronounced plasmonic resonances. Chiral molecules such as cysteines (44), peptides (45–48), and DNA (49) can be bound to the surfaces of metal particles by noncovalent or covalent interactions. The chiroptical responses of the complexes can be precisely tuned through rational control of the chiral ligands on the particle surfaces (50, 51). For instance, di Gregorio et al. (52) reported Ag nanocubes capped with glutathione, showing drastic CD changes upon slightly lowering the pH from 5 to 4.5 (see **Figure 2*a***). A chemical effect of catalyzing the formation of diglutathione took place at lower pH, resulting in such CD changes. In addition, the orientations of the chiral ligands on the particle surfaces can also have a significant impact on the chiroptical properties. Lu et al. (53) demonstrated discrete Au/Ag core-shell nanocubes surface functionalized with DNA. The authors studied molecular alignment effects of the DNA on the particle surfaces by changing the ionic strength of the solution. When the ionic strength was 0 (deionized water), a plasmon-induced CD of approximately 5 mdeg was observed. In this case, the authors interpreted that the DNA molecules were aligned perpendicular to the particle surfaces owing to their electrostatic repulsion. In contrast, when the salt concentration was increased, the resulting random DNA orientations led to the observed gradual decrease of the CD responses. When the ionic strength was increased using 0.1 M PBS, the resulting CD value was less than 0.5 mdeg and could hardly be identified.

Plasmon-induced chirality can be effectively enhanced when the chiral ligands are in close proximity to the particle surface (33). In a newly developed strategy, chiral ligands have been embedded within core-shell structures through multistep metallization processes. For example, Hou et al. (54) optimized the optical chirality of cysteine-modified AuNRs via Ag coating. The entrapment of cysteines at the Au–Ag interface amplified the localized electromagnetic fields around the ligands, producing a large enhancement of the CD responses from no obvious signals to nearly 60 mdeg. Lan & Wang (55) demonstrated a similar approach with Ag shell coating on DNA-capped AuNRs. In these morphologically diverse core-shell structures, the plasmon-induced CD was readily manipulated over a broad spectral range by simply controlling the shape anisotropy of the building blocks. Wu et al. (56) reported hybrid Au core–DNA–Ag shell nanoparticles with strong and tunable CD using cytosine-rich single-stranded DNA as a guiding template for subsequent Ag shell growth, in which the largest CD value could reach more than 100 mdeg (see **Figure 2*b***). In another work (57), authors from the same group fabricated Au–gap–Ag quasi-spherical architectures with interior nano-bridged gaps filled with cysteines (see **Figure 2*c***). The plasmon-induced CD from the structures was tailored by carefully adjusting the nanogap distance and ligand density.

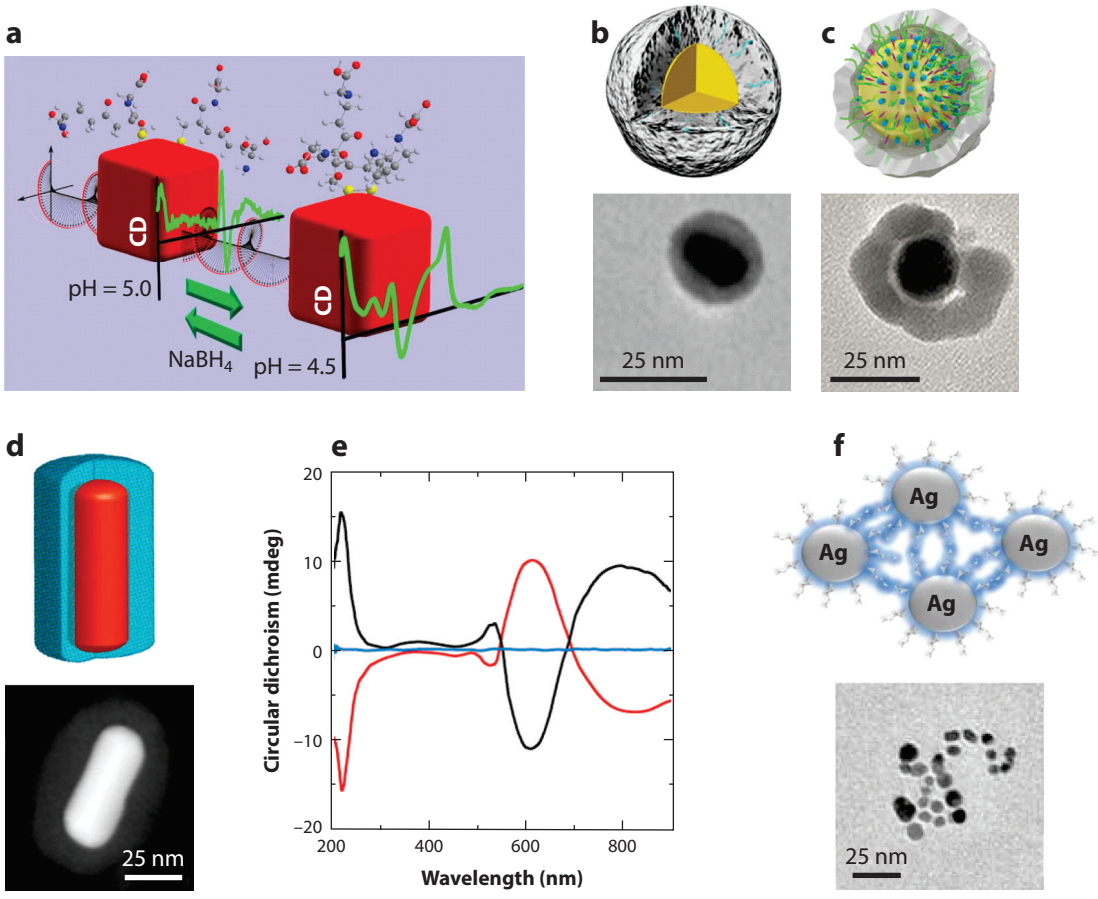

Figure 2

Plasmon-induced chirality arising from the interactions between chiral molecules and achiral plasmonic nanoparticles. (*a*) Ag nanocubes capped with glutathione. (*b*) Au core–DNA–Ag shell nanoparticles. (*c*) Au–gap–Ag quasi-spherical structures with nanogaps filled with cysteines. (*d*) Au nanorod-chiral mesoporous silica core-shell structures. (*e*) Optical response of the structures shown in *d*. (*f*) Cholate-coated Ag nanoparticle networks. Panel *a* adapted with permission from Reference 52. Panel *b* adapted with permission from Reference 56. Panel *c* adapted with permission from Reference 57. Panels *d* and *e* adapted with permission from Reference 59. Panel *f* adapted with permission from Reference 63.

Apart from organic and biological chiral molecules, inorganic chiral materials can also couple with metal nanoparticles to form hybrid complexes (58). Liu et al. (59) showed a typical example by coupling chiral mesoporous silica (CMS) with AuNRs, as shown in **Figure 2*d*,*e***. The authors synthesized AuNR–CMS core-shell structures with distinct CD signatures in the visible spectral range, the intensities of which could reach more than 10 mdeg (see **Figure 2*e***), arising from the interactions between the AuNRs and the chiral molecules in the mesopores of the silica shells.

Besides discrete nanostructures, plasmon-induced chirality has also been achieved in large assemblies in which nanoparticles were linked together by chiral molecules (60, 61). For instance, Zhu et al. (62) created 1D assemblies of cysteines and AuNRs. More specifically, cysteine molecules were attached at the ends of the NRs and linked them together to form assemblies. In another example, Layani et al. (63) reported nanostructures composed of crosslinked cholate-coated Ag nanoparticles, illustrated in **Figure 2*f***. In this case, the observed CD was induced owing to the

cholate molecules placed in the regions between the nanoparticles, where the plasmonic near-fields were localized. Kneer et al. (64) studied the role of the interparticle distance on CD transfer efficiency. The authors assembled Au and Ag nanoparticles on DNA origami, which allowed for precise tuning of structural geometries. It is noteworthy that large assemblies created by chiral molecule–linked plasmonic nanoparticles may also exhibit pure plasmonic chirality, resulting from the handed arrangements of the metal particles. The CD responses associated with plasmonic chirality occur at similar spectral positions and in general are much stronger than plasmon-induced chirality (65), thus making the latter difficult to differentiate.

3. INTRINSICALLY CHIRAL COLLOIDS

Chiroptical responses can also be generated from metal nanoparticles that are intrinsically chiral. When interacting with light, the excited plasmonic modes can span the entire chiral nanoparticle**.** Therefore, the CD strength and line shape can be readily manipulated by tuning the geometry of the particle itself. **Figure 3*a*** depicts an interesting example studied theoretically. A spherical particle is deformed with a ridge running in a spiral fashion around the particle surface (41). Similarly, one can create a spiral slit cut into the particle. Such a structure is called a twister, and its counterpart is called an antitwister. The chiroptical responses arise from the mixing of the particle plasmon modes of different orders arising from rather small geometrical distortions. The mode formation is complex and sensitively depends on the particle geometry. In general, the resulting chiroptical responses are quite weak if the geometrical distortions are small.

One can increase the chiroptical responses by introducing larger particle deformations. **Figure 3*b*** shows experimental CD data from plasmonic nanohelices (66). The nanohelices were fabricated using a sophisticated evaporation scheme, called glancing angle deposition, which allowed for creation of high-quality chiral plasmonic structures with full control over handedness and geometric properties. The excited plasmonic modes had a very strong chiral nature. The measured CD spectra underpinned this expectation. A molar ellipticity of $\sim 10^9$ $(\text{M cm})^{-1}$ was determined experimentally. Excellent mirror symmetry for left- and right-handed (LH and RH) nanohelices was observed, as shown in **Figure 3*b***. A strategy to synthesize chiral Au nanoparticles in the presence of amino acids and peptides was developed recently (see **Figure 3*c***) (67). The synthesis was based on enantioselective interactions between the inorganic surfaces and the chiral molecules, which led to the formation of kink sites in the nanoparticles during growth. Well-tailored chiroptical responses were observed, as shown in **Figure 3*d***, with CD values in the range of 0.5 deg.

Enantioselective control of lattice and shape chirality could also be achieved in inorganic nanostructures made of tellurium (68). The chiroptical responses of these tellurium nanocrystals were from two origins, atomic lattice and mesoscale shape. First, the tellurium nanocrystals were of a chiral atomic space group, either $P3_121$ or its enantiomorph, $P3_221$. Second, the overall chiral shapes could be controlled in the presence of chiral biomolecules, for example, cysteine or glutathione, leading to CD responses on the order of 30 mdeg. The authors inferred that the chiroptical responses mainly originated from the shape of the nanoparticle and that the crystal structure played a secondary role. The chiroptical responses could be further amplified by using the tellurium structures as templates to deposit Ag or Au.

4. PLASMONIC CHIRALITY

4.1. Theoretical Background

Plasmonic nanostructures composed of individual nanoparticles arranged in chiral geometries can exhibit strong plasmonic chirality in the visible and near-infrared spectral regions (69). **Figure 4*a***

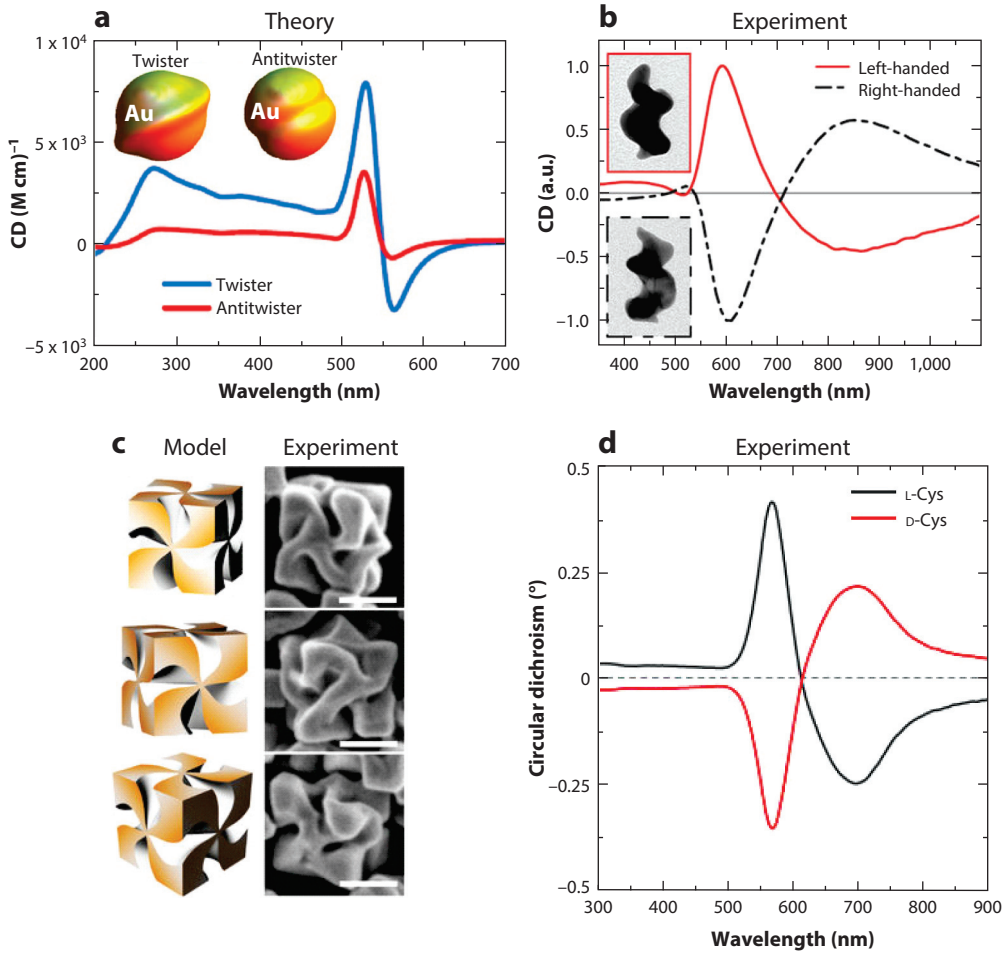

Figure 3

Intrinsically chiral colloids. (*a*) Sketch as well as theoretical circular dichroism (CD) spectra for chiral Au nanocrystals: twister and antitwister. (*b*) Experimental CD spectra of Au nanohelices. (*Inset*) Transmission electron microscopy images of the left-handed (*top*) and right-handed (*bottom*) Au helices (image dimensions: 85 nm × 120 nm). (*c*) Three-dimensional models (*left*) and corresponding electron micrographs (*right*) of helicoid Au particles. All scale bars are 100 nm. (*d*) CD spectra of the Au helicoids synthesized in the presence of L-cysteine (Cys) (*black*) and D-Cys (*red*), respectively. Panel *a* adapted with permission from Reference 41. Panel *b* adapted with permission from Reference 66. Panels *c* and *d* adapted with permission from Reference 67.

shows an example of such systems. Spherical and thus achiral nanoparticles are organized in a helical frame. The plasmonic modes of the individual particles interact via their respective electromagnetic fields to generate collective modes of the entire structure. The dipolar limit applies when the size of the metal nanoparticle a is smaller compared with the interparticle distance R. In this case, the resulting plasmonic CD obeys the following relation (69):

$$\mathrm{CD}_{\text{plasmon-plasmon}} \propto a^{12}/R^{8}. \qquad 5.$$

These high power orders clearly elucidate that the strength of the plasmonic CD significantly depends on the nanoparticle size and the distance between them. **Figure 4*b*** shows the calculated CD spectra of nanohelices with different numbers of nanoparticles in water. These CD signals

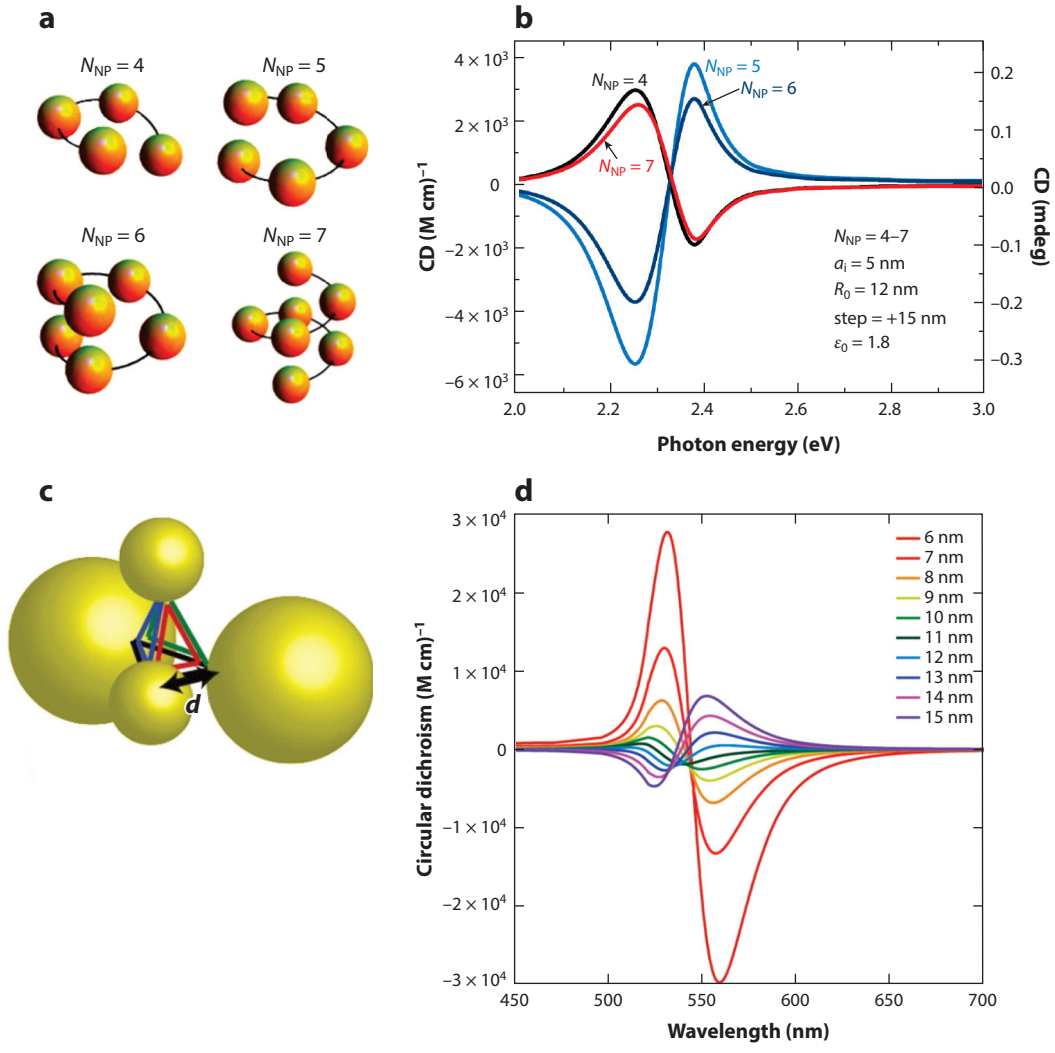

Figure 4

Theoretical circular dichroism (CD) calculations of chiral plasmonic assemblies. (*a*) Schematic of a helical arrangement of spherical Au nanoparticles (NPs). (*b*) Calculated CD spectra of the helical Au nanoparticle assemblies in dependence on the particle number. (*c*) Schematic of a tetrahedral arrangement with four Au nanoparticles of two different sizes. Symmetry breaking by changing the distance *d* along one edge of the tetrahedral frame renders the overall structure chiral. (*d*) Calculated CD spectra for different distance *d* values as indicated in panel *c*. Distance changes of a few nanometers can invert the handedness of the structure and thus the CD responses. Panels *a* and *b* adapted with permission from Reference 69. Panels *c* and *d* adapted with permission from Reference 73.

are averaged-over orientations of the nanohelices. Clear bisignate spectral profiles are observed. Interestingly, the sign of the bisignate shape can be largely influenced by the number of particles in the helix. At first sight, this is counterintuitive, as the handedness of the plasmonic helices does not change, and thus the sign should not change. However, when the particle number in each nanohelix is small, the sign of the bisignate shape in the orientation-averaged spectra can be very sensitive to the particle number, shape, and size of the helix if the helix has a relatively short pitch (69). In fact, the CD spectrum can flip with addition of just one nanoparticle (see **Figure 4*b***).

This results from the formation of hot spots between some of the nanoparticles in the helical assembly with a relatively small pitch (69). When the pitch of the plasmonic helix is comparable with its diameter, the flipping of sign of the CD may not appear, and the CD signal can be stable as the number of nanoparticles in the helix increases (70, 71). Plasmonic CD in the tetrahedral and pyramidal assemblies of four nanoparticles was also critically dependent on the details of the structures (72).

Figure 4*c* presents another interesting chiral arrangement. Here, four spherical particles of two different sizes are organized in an asymmetric tetramer frame (73). In contrast to the particle helices shown in **Figure 4*a***, the handedness of the tetramer structure is less obvious and is caused by a shift of the lower smaller particle out of the symmetric position, therefore breaking mirror symmetry. What is interesting in this configuration is the possibility to invert the handedness of the structure via subtle conformation changes. As long as the lower small particle crosses the mirror plane, the handedness of the structure flips, and so does the sign of the bisignate shape of the CD responses (**Figure 4*d***). In this case, the sign of the CD spectrum is indeed an indication of the structure handedness.

4.2. Experimental Realizations

In this section, we discuss various experiments conducted using different self-assembly techniques, including chiral templates, self-assembly with discrete DNA strands, and DNA origami templates.

4.2.1. Chiral templates. Templating is one powerful strategy to organize metal nanoparticles into chiral plasmonic assemblies (74–79). Useful chiral templates, including biomacromolecules (80–82) and polymers (83–86), can be exploited to pattern a variety of plasmonic building blocks to achieve chiral nanostructures (87–89). In general, the template-guiding scheme can produce large-scale plasmonic nanostructures with strong chiral responses. In some cases, the contribution owing to plasmon-induced chirality from interactions between the chiral templates and metal nanoparticles, as discussed in Section 2, might also be present (65). In other words, the resulting CD often possesses a complex origin from both exciton–plasmon and plasmon–plasmon interactions. However, in most cases, the overall chiroptical responses are dominated by plasmonic chirality owing to its much larger strength compared with that of plasmon-induced chirality (details can be found in the theoretical discussion in Sections 2.1 and 4.1). In the following, we thus focus only on the contribution from plasmonic chirality.

Rosi's group (90–94) reported peptide-templated chiral assembly of Au nanoparticles and constructed a series of helical superstructures. In the first step, rationally designed peptides were assembled to form chain-like helices as frameworks. Au nanoparticles were then synthesized at the Au-binding sites on the peptides via in situ reduction. The conjugation sites played a dual role in this methodology: anchoring the Au species for Au nanoparticle nucleation and growth and directing the helical assembly of the as-formed Au nanoparticles. Both LH and RH double-helical arrays with tunable particle sizes were obtained via alteration of the peptide templates and reduction conditions. Strong and tunable CD signals were observed from these superstructures. The experimental procedure was further optimized in recent work shown in **Figure 5*a*** (95). Chemical modification of the conjugation sites led to the formation of Au nanoparticle single-helical arrays, which exhibited the highest CD responses among the peptide-directed assemblies.

Another template with organogelators has also been widely exploited for in situ preparation of chiral plasmonic nanostructures (96, 97). In coordination with noble metal ions such as Au(III) and Ag(I), the designed organogelators were turned into gels through a sol-gel transition process. Au and Ag chiral superstructures and large-scale films templated by the gels were formed by

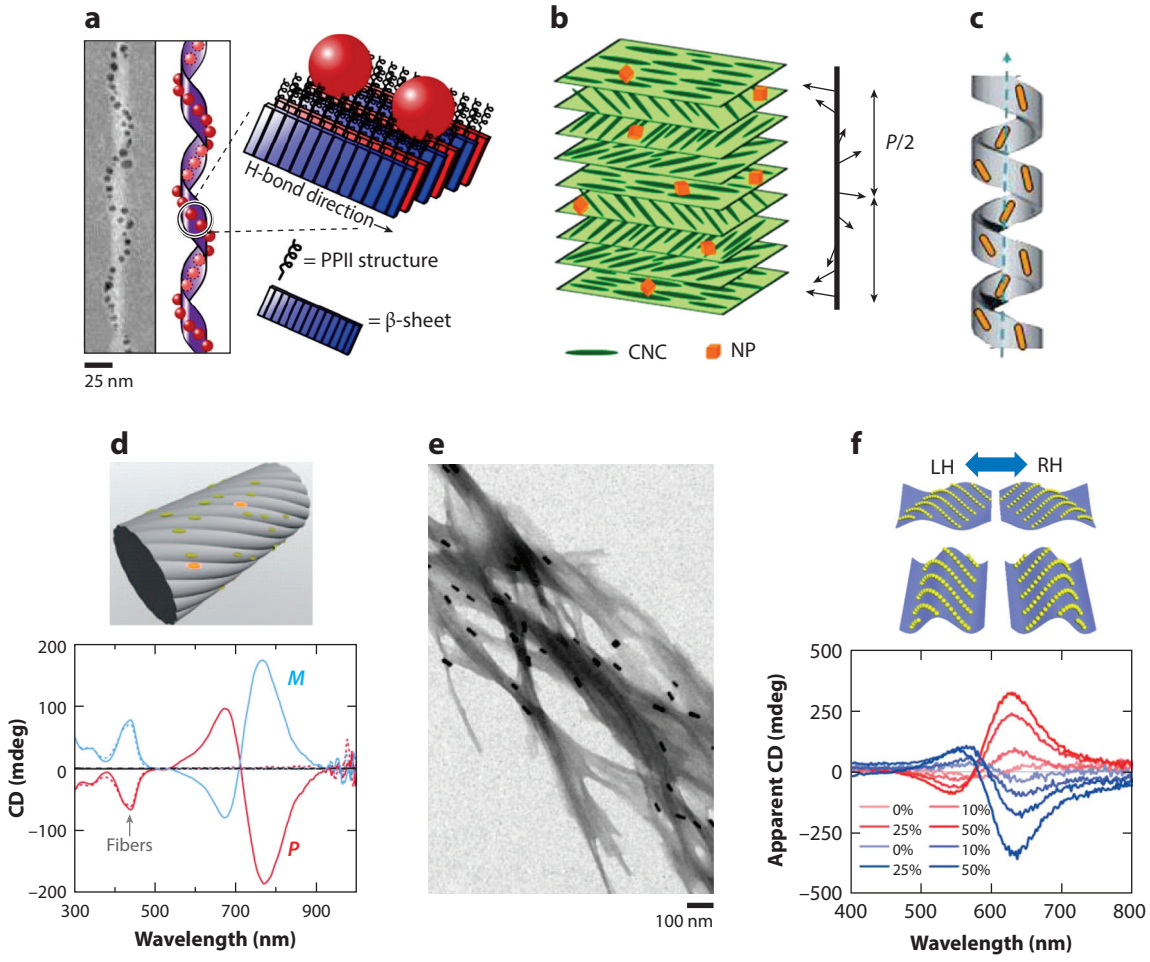

Figure 5

Templated chiral plasmonic structures. (*a*) Single-helical arrays of Au NPs templated by peptides. (*b*) Au nanocubes loaded on chiral films of cellulose nanocrystals. (*c*) Hybrid structures of AuNRs with CTAB and lipids. (*d*) CD spectra of the AuNR superstructures templated by twisted supramolecular fibers. (*e*) Transmission electron microscopy image of the chiral AuNR superstructures shown in panel *d*. (*f*) Chiral nanocomposites consisting of layer-by-layer-assembled Au NP films coated on macroscale twisted poly(dimethylsiloxane) substrates. The NP films can be reconfigured by stretching, leading to distinct optical responses in the CD spectra that strongly depend on the stretching directions. Abbreviations: CD, circular dichroism; CNC, cellulose nanocrystal; LH, left-handed; NP, nanoparticle; NR, nanorod; PPII, polyproline II; RH, right-handed. Panel *a* adapted with permission from Reference 95. Panel *b* adapted with permission from Reference 114. Panel *c* adapted with permission from Reference 115. Panels *d* and *e* adapted with permission from Reference 116. Panel *f* adapted with permission from Reference 117.

subsequent in situ reduction of the ions. In addition, CMS, a more rigid template, was used for the synthesis of chiral plasmonic materials (98–101). Xie & Che (102) reported Ag nanowire arrays supported by CMS with a distinct multihelix through in situ synthesis in the mesopores, which possessed distinct CD responses originating from the interactions between the Ag nanowires.

The as-synthesized metal nanoparticles can also be directly absorbed onto chiral templates. In particular, liquid crystalline polymers offer a broad family of such templates that can be used to efficiently guide the construction of chiral plasmonic assemblies (103–106). Cellulose

nanocrystals, which show rodlike morphologies, are considered as representative materials among them (107). For example, a chiral nematic phase with orientational order was formed via aggregation of the anisotropic cellulose nanocrystals. Thin films of these cellulose nanocrystals offer host sites for assembling guest nanoparticles with orientational control (108–110). After the introduction of plasmonic building blocks, the host–guest composites showed distinct CD, much stronger than that from the templates themselves. Chu et al. (111) reported Au nanoparticle chiral assemblies loaded on free-standing cellulose nanocrystal films. These host–guest composites exhibited not only tunable and switchable CD responses but also unique angle-dependent plasmon resonance properties. Moreover, ultralong Ag nanowires were used as building blocks (112). The authors realized tunable chiral distribution of the aligned Ag nanowires with long-range order through the cellulose nanocrystal liquid crystal–mediated realignment. It is noteworthy that chiral organizations of anisotropic nanoparticles such as nanowires and NRs usually display more pronounced CD responses when compared with their spherical counterparts, owing to their larger resonance dipole moments. Querejeta-Fernández et al. (113) demonstrated a similar system, in which AuNRs were loaded on cellulose nanocrystal films to generate chiral plasmonic complexes.

Later, the authors tuned the chiroptical properties using AuNRs with different aspect ratios and different types of cellulose nanocrystals, as shown in **Figure 5*b*** (114). Nanocubes containing octahedral Au cores and Ag shells were integrated in these chiral films as well. Apart from cellulose nanocrystals, other cholesteric liquid crystals were also used as chiral templates. Wang et al. (115) reported an AuNR/CTAB/lipid, a chiral hybrid superstructure in which the AuNRs were well dispersed on a CTAB/lipid supramolecular template (see **Figure 5*c***). Strong chiral responses were achieved owing to the helical alignment of AuNRs in the CTAB/lipid nanoribbons. Similar to a molecular liquid crystalline phase, helical geometries of the AuNR superstructures and the resulting CD responses showed interesting temperature dependence.

Expanding the scale of the plasmonic assemblies is an efficient approach for acquiring stronger CD, as more intense coupling effects can take place among the metal nanoparticles. As shown in **Figure 5*d***, Liz-Marzán's group (116) demonstrated AuNR superstructures templated by chiral fibers. Specifically, AuNRs were adsorbed onto the supramolecular fiber scaffolds with twisted morphologies through particular noncovalent interactions to form 3D helical ordering. These remarkable composites possessed lengths of up to micrometers. The AuNRs on the fibers were strongly coupled owing to their nearly end-to-end arrangement. As a result, giant chiral responses, as well as unprecedented levels of anisotropy factors from the visible to the near-infrared regime, were observed from the superstructures (see **Figure 5*e***). Additionally, the CD signals and the anisotropy factors of the composites could be precisely tailored via tuning of the AuNR concentration. In a recent work, Kim et al. (117) realized chiral plasmonic composites using macroscale templates (see **Figure 5*f***). Exploited as templates, macroscale elastic poly(dimethylsiloxane) substrates were conformally coated with layer-by-layer-assembled Au nanoparticle films. The substrates were mechanically twisted in opposite directions to form LH and RH structures, respectively. The chiral responses could be reversibly reconfigured and cyclically modulated through mechanical stretching. The layered composites of Au nanoparticles exhibited strong CD with values up to 300 mdeg, showing distinct features around the plasmonic resonance positions.

4.2.2. Self-assembly with discrete DNA strands. Among a variety of materials for self-assembly, DNA is one of the most attractive candidates owing to its high degree of programmability and sequence specificity. The research field of structural DNA nanotechnology makes use of the highly sequence-specific interactions between complementary DNA strands to create DNA

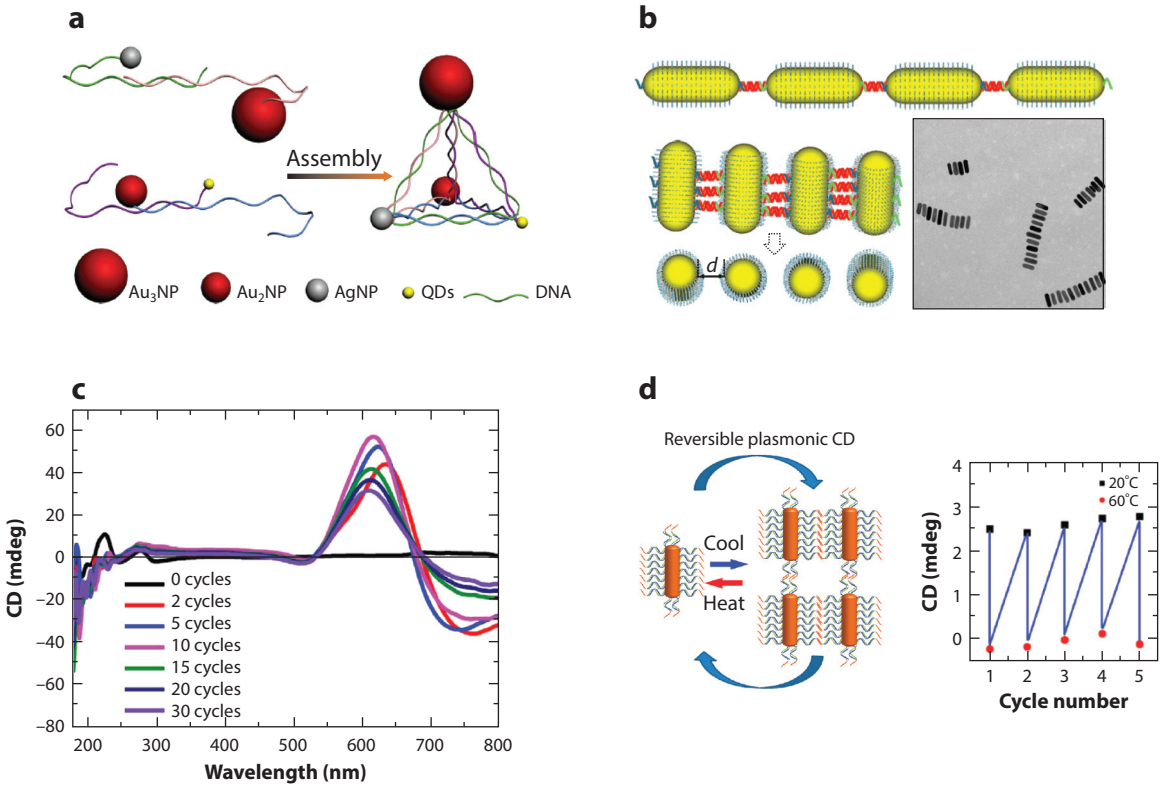

Figure 6

Chiral plasmonic nanostructures assembled with discrete DNA strands. (*a*) Pyramidal structure consisting of four different NPs. (*b*) AuNRs assembled through polymerase chain reaction. (*c*) Optical responses of the side-by-side-assembled AuNRs. (*d*) Temperature-controlled AuNR assembly and disassembly. Abbreviations: CD, circular dichroism; NP, nanoparticle; NR, nanorod; QD, quantum dot. Panel *a* adapted from Reference 118; panels *b* and *c* adapted from Reference 27; panel *d* adapted from Reference 119.

nanostructures that can be programmed in a rational manner. This has allowed for the realization of chiral plasmonic nanostructures assembled by discrete numbers of DNA strands. In such assemblies, the distances among the particles can be tuned by the lengths of the DNA linkers.

Kotov and coworkers (118) demonstrated pyramidal groupings of four different constituents including two Au nanoparticles, one Ag nanoparticle, and a quantum dot using DNA (**Figure 6*a***). By precisely controlling the DNA strand number on the particles, Au nanoparticle dimer formation was achieved with high yield. In a second step, pyramids with four different constituents were assembled out of two nanoparticle dimers. Introduction of constituents with different sizes led to symmetry breaking. The structures displayed CD responses in the visible spectral range. The three different features in the CD spectrum from 350 to 550 nm could be attributed to the plasmonic excitations of the Au and Ag nanoparticles and the optical transitions of quantum dots. In addition, Kotov and coworkers (27) developed a protocol based on polymerase chain reaction to detect attomolar concentrations of DNA via CD spectroscopy. AuNRs were modified with DNA primers and acted as monomers or building blocks for the assembly of chiral nanostructures. The polymerase chain reaction was used to elongate the primers, which were then able to form larger assemblies. By controlling the DNA-primer modification on the AuNRs to be at either the AuNR ends or sides, the authors showed either end-to-end or side-by-side assembly of

the AuNRs (**Figure 6*b***). Side-by-side-assembled structures showed optical activity (**Figure 6*c***). Twisting of the AuNRs with respect to each other broke the symmetry of the parallel assemblies. As a result, clear CD signals were observed from the dimers with values up to 60 mdeg. The enantiomeric preference was due to the twisting of the DNA linkers as well as the minimal energy conformation of the two charged AuNRs, which were nonparallel.

In 2012, Li et al. (119) demonstrated reversible switching of plasmonic CD by thermal control (**Figure 6*d***). The chiral structures were formed by AuNRs upon cooling and disassembled into individual AuNRs upon heating. With this approach the authors showed a simple strategy to switch plasmonic CD. However, the number and orientations of the AuNRs in the assembly were not controllable. Wu et al. (120) realized a well-defined structure switching based on geometrical reconfiguration of the linker strands. The authors engineered a propeller-like chiral tetramer of four nanoparticles: a central upconversion nanoparticle surrounded by three AuNRs. The distance between the upconversion nanoparticle and the AuNRs was tuned via DNA hairpins in the linker strands that could be opened and closed. The fluorescence and chiropical response of the system were highly controllable. Assembly with discrete DNA strands is a successful strategy to assemble chiral plasmonic structures with a small number of particles. Nevertheless, the complexity of the structures that can be assembled by this approach is still limited.

4.2.3. DNA origami templates. The breakthrough in structural DNA nanotechnology came with a concept called DNA origami, which involves the folding of a long DNA scaffold strand by hundreds of designed short oligonucleotides (121). The so-called staple oligonucleotides are hybridized to the DNA scaffold through Watson–Crick base pairing to create arbitrary 2D or 3D nanostructures. Because the positions of the staples within the DNA origami are predetermined, the formed DNA nanostructure is fully addressable. Functionalization of DNA origami is enabled by capture strands that extend from the DNA origami. This allows for DNA origami assembly of metal nanoparticles, quantum dots, fluorescent dyes, and other entities. Compared with other assembly strategies based on discrete DNA strands (27, 118–120, 122–128), the DNA origami approach offers several major advantages. The folding is more robust against imperfections in the stoichiometry of the individual DNA strands, and the formed DNA origami template is more rigid, enabling nanoparticle assemblies with defined configurations.

Yan and coworkers (129) were the first to assemble multiple Au nanoparticles on DNA origami, which has inspired researchers to step beyond simple plasmonic geometries such as dimers and trimers. In 2012, Kuzyk et al. (71) demonstrated the experimental realization of chiral plasmonic nanostructures. The authors created Au nanoparticle helices that exhibited designated chiroptical properties. The Au nanoparticles were wound around a rigid DNA origami bundle in both handednesses (**Figure 7*a***). The helical arrangements of the Au nanoparticles gave rise to characteristic bisignate CD spectra centered at the resonance frequency of the individual nanoparticles (**Figure 7*b***). To increase the CD signal strength, electroless metal depositions with Ag and Au were carried out. CD signals up to 150 mdeg were achieved. This corresponds to a molar CD of $\sim 10^8$ $(M\ cm)^{-1}$, which is still one order smaller than the CD responses obtained from the nanohelices in **Figure 3*b***. Shen et al. (130) also demonstrated the formation of Au nanoparticle helices using DNA origami. A 2D rectangular DNA origami was first used to organize Au nanoparticles precisely at well-defined binding sites along two linear chains. Au nanoparticle helices were then achieved by rolling and stapling the origami sheets into tubes.

Shen et al. (131) provided a detailed study of the essential ingredients for achieving strong plasmonic chirality. The authors used a rigid addressable DNA origami template to precisely organize four nominally identical Au nanoparticles into a 3D asymmetric tetramer. They demonstrated that both structural asymmetry and plasmonic resonant coupling were required for achieving

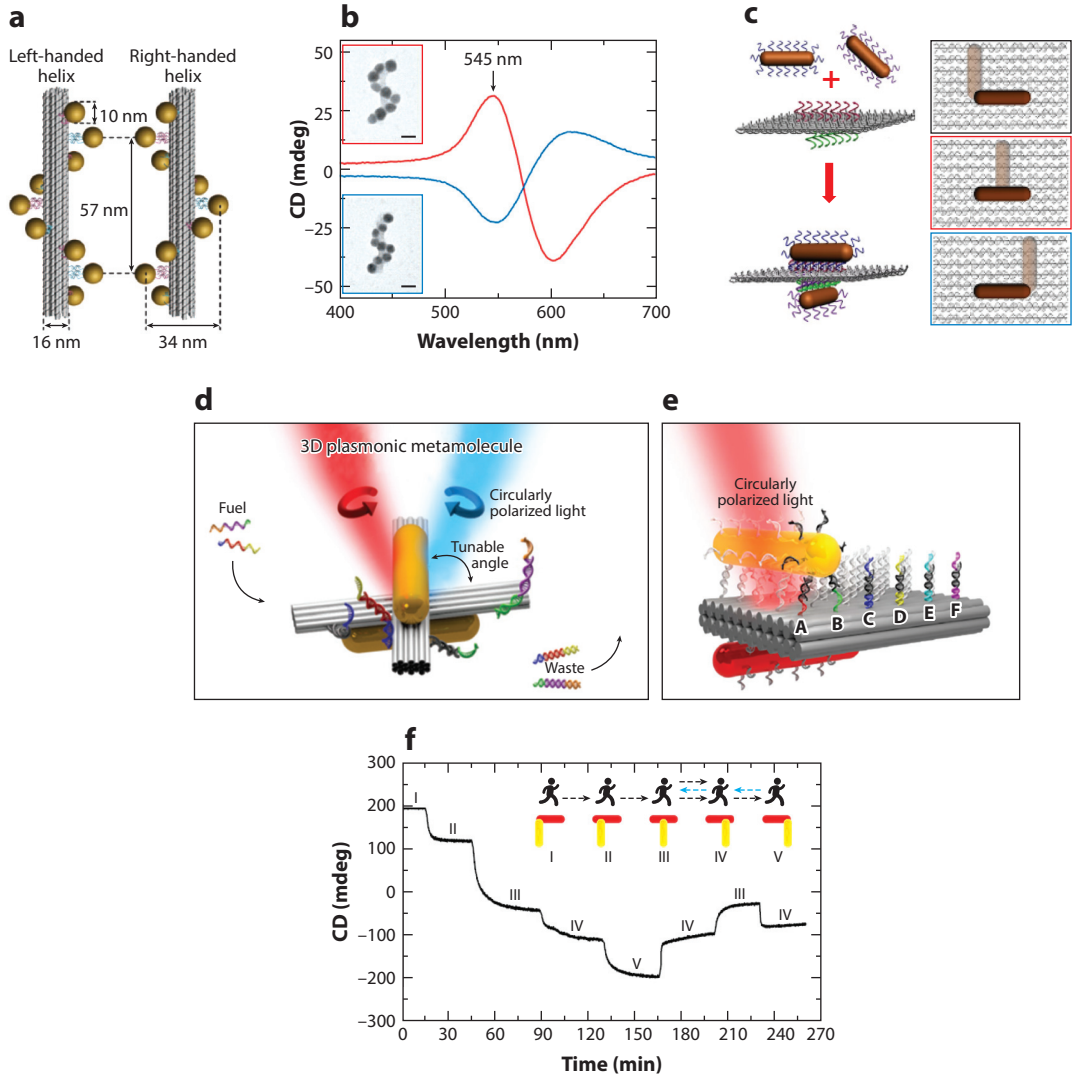

Figure 7

Chiral plasmonic nanostructures templated by DNA origami. (*a*) Schematic of nanoparticle helices. (*b*) Experimental circular dichroism (CD) spectra and transmission electron microscopy images of the helices (scale bars are 20 nm). The left-handed and right-handed helices show clear CD responses in the visible wavelength range. (*c*) Different arrangements of gold nanorod (AuNR) dimers assembled on rectangular DNA origami. The assembly strategy allows for straightforwardly creating left-handed, right-handed, and achiral structures. (*d*) Schematic of a 3D reconfigurable plasmonic metamolecule consisting of two NRs on a DNA origami template. (*e*) Schematic of a plasmonic AuNR walker assembled on rectangular DNA origami. The lower NR is immobilized, whereas the upper one can walk over the origami sheet upon addition of the appropriate DNA strands. (*f*) In situ monitoring of the walking process. (*inset*) The numbers I–V represent different states of the system. Panels *a* and *b* adapted with permission from Reference 71. Panel *c* adapted with permission from Reference 139. Panel *d* adapted with permission from Reference 146. Panels *e* and *f* adapted with permission from Reference 149.

strong chiral responses. DNA origami also enabled chiroptical responses from centrosymmetric octahedral DNA frames (132). In this case, the Au nanoparticles were arranged at prescribed locations on the vertices of the frame. The CD responses resulted from the use of different-sized nanoparticles organized in an octahedral heterocluster. Later, Urban et al. (133) also investigated the assembly of multiple chiral building blocks into more complex chiral architectures. They demonstrated hierarchical assembly of plasmonic toroidal metamolecules consisting of four identical DNA origami–templated helical building blocks. Plasmonic toroidal metamolecules showed stronger chiroptical responses than the constituent building blocks, including helical monomers and dimers.

Compared with spherical nanoparticles, anisotropic AuNRs possess stronger resonant dipole moments and more efficient spectral tunability (134). In addition, it is possible to create a 3D chiral nanostructure using only two identical AuNRs (135–138). Nevertheless, assembly of AuNRs on DNA origami with a high yield is considerably more challenging than assembly of isotropic nanoparticles, which are not orientation dependent. Lan et al. (139) reported AuNR crosses with controlled interparticle distance and spatial orientations on rectangular bifacial DNA origami (see **Figure 7*c***). Tuning the docking positions of the AuNRs allowed for the realization of LH and RH plasmonic nanostructures. The authors subsequently demonstrated helical AuNR superstructures with tailored plasmonic chirality in a programmable manner (140). By designing the arrangement pattern of the DNA capture strands on both sides of a 2D DNA origami template, AuNRs were assembled into NR helices with intercalated origami. LH and RH AuNR helices were fabricated by tuning the mirrored-symmetric patterns of the capture strands on the origami.

Efforts have also been devoted to controlling the positions of single-stranded DNA on Au nanoparticles (141). Zhang et al. (142) recently combined the advantage of the DNA origami technique and the assembly strategy of discrete DNA strands. By attaching an Au nanoparticle to a set of patterned DNA strands on origami, the positions of the strands on the Au nanoparticle could be controlled. Subsequent detachment of the modified Au nanoparticle allowed for assembly with additional Au nanoparticles to form chiral plasmonic nanostructures. The authors demonstrated great control over the chirality of pyramidal nanoparticle groupings.

The most unique feature of the DNA origami technique lies in the possibility to reconfigure the assembled plasmonic architectures (143–145). This gives rise to dynamic optical responses. Compared with the systems shown in **Figures 5*f*** and **6*d***, the DNA origami–based dynamic structures offer greater control over geometrical reconfigurations. When designing dynamic nanoscale devices, three important requirements must be considered. First, an efficient energy input for triggering reconfiguration of the device is crucial. Second, the reversibility of the conformational changes should be ensured. Last but not least is the ability to monitor the nanoscale reconfiguration and to translate it into tailorable functionalities. Kuzyk et al. (146) demonstrated reconfigurable chiral plasmonic nanostructures, which executed DNA-regulated conformational changes at the nanoscale (see **Figure 7*d***). Owing to their strong optical response and anisotropic nature, AuNRs are excellent candidates for the realization of plasmonic architectures with distinct and tailored optical functionalities. By adding specifically designed DNA fuel strands, the plasmonic nanostructures could be switched between different conformational states characterized by distinct CD spectra. The same authors also extended the concept to realize a light-driven chiral plasmonic system (147). Kuzyk et al. (148) recently reported the realization of chiral plasmonic nanostructures, which could respond to a wide range of pH changes. The introduction of pH-sensitive DNA locks as active sites allowed for selective reconfiguration of different plasmonic species coexisting in solution through simple pH tuning.

Zhou et al. (149) demonstrated a chiral plasmonic system in which an AuNR could perform stepwise walking directionally and progressively on DNA origami (see **Figure 7*e***). The nanoscale

steps were in situ monitored by CD spectroscopy (see **Figure 7*f***). The key idea was to design a plasmonic coupling scheme in which a walker and a stator constituted a conformationally sensitive geometry. In the plasmonically coupled system, the stepwise movements of the AuNR walker triggered immediate spectral responses that could be tracked optically. This design enabled the discrimination of stepwise walking with step size far below the optical diffraction limit in real time. Urban et al. (150) further advanced the system and showed a plasmonic walker couple system, in which two NR walkers could independently or simultaneously perform stepwise walking powered by DNA hybridization along the same DNA origami track to achieve dynamic chiral response changes.

5. CONCLUSIONS AND OUTLOOK

We have summarized recent advances in the field of chiral plasmonic nanostructures created via synthesis methodologies. First, localization of chiral molecules in close proximity to achiral metal nanoparticles can lead to plasmon-induced chirality, shifting the observation window of molecular CD from the UV to visible frequencies while simultaneously enhancing its strength. Plasmon-induced chirality is very sensitive to the orientation of the molecules with respect to the metal particle surfaces. Thus, random orientations of molecules attached to metal nanoparticles may result in diminishing CD. This calls for more comprehensive theoretical understanding to select appropriate chiral molecules, as well as to identify optimized placement and orientation of the molecules on the particle surfaces. Simultaneously, this also fuels the urge to further develop chemical synthesis schemes to control the placements and orientations according to the theoretical blueprints. Plasmon-induced chirality is suited to optically probe attachment of biological molecules, such as proteins and DNA, for in situ structural determination, chiral sensing, and recognition or separation of chiral molecules.

Second, advanced synthesis strategies have enabled the realization of intrinsically chiral colloids. Such nanoparticles possess chiroptical responses that can be tuned by manipulating their shapes and sizes. The resulting CD is thus a very sensitive tool to characterize the morphology and size dispersion of the 3D nanostructures in a solution. Again, understanding the origin of chirality in such colloidal particles is very beneficial to further explore the applications of chiral particles for, e.g., chiral analysis and separation.

Third, the assembly of achiral metal nanoparticles into chiral plasmonic nanostructures follows two major routes. One lies in the attachment of metal particles on chiral hosts, e.g., peptides, nanocrystalline cellulose, surfactant mixtures, or polymeric films. Although control over structural geometries is limited, this approach allows for production of chiral plasmonic materials of large quantities. However, more endeavors must be carried out to achieve well-controlled and better-defined structural morphologies for high-yield preparation and the possibility of scalable synthesis. On the other hand, DNA self-assembly offers tremendous control over structural geometries, as well as accurate positioning of metal nanoparticles in chiral frames. In particular, dynamic DNA nanotechnology enables 3D reconfiguration of plasmonic nanostructures, giving rise to dynamic chiral response changes. Such chiral plasmonic architectures can be engineered to undergo geometrical reconfiguration triggered by a wealth of stimuli, thus enabling a new route for dynamic sensing of molecules and entities. With a proven set of theoretical modeling tools and a variety of successful synthetic approaches, the field of chiral plasmonics is in a promising position to create solutions to long-standing challenges in enantioselective catalysis, ultrasensitive detection of multiple disease biomarkers, and optical monitoring of transmembrane transport and intracellular metabolism.

DISCLOSURE STATEMENT

The authors are not aware of any affiliations, memberships, funding, or financial holdings that might be perceived as affecting the objectivity of this review.

ACKNOWLEDGMENTS

N.L. was supported by the Sofja Kovalevskaja Award from the Alexander von Humboldt Foundation, the Volkswagen Foundation, and a European Research Council (ERC Dynamic Nano) grant. M.J.U. acknowledges financial support from the Carl-Zeiss-Stiftung. X.-T.K. was supported by the China Postdoctoral Science Foundation (2015M580778). X.-T.K. and A.O.G. were supported by the Volkswagen Foundation. A.O.G. is a Chang Jiang (Yangtze River) Chair Professor of the Government of China. A.O.G. also acknowledges Sichuan Province for a Thousand Talents short-term award. Q.W. thanks the National Natural Science Foundation of China for financial support (grants 21425103 and 21673280). M.H. acknowledges funding from ERC (COMPLEXPLAS), MWK Baden-Württemberg (ZAQuant, IQST), DFG (SPP1839), and BW Stiftung (Proteinsens).

LITERATURE CITED

1. Kelly KL, Coronado E, Zhao LL, Schatz GC. 2003. The optical properties of metal nanoparticles: the influence of size, shape, and dielectric environment. *J. Phys. Chem. B* 107:668–77
2. Stockman MI. 2011. Nanoplasmonics: past, present, and glimpse into future. *Opt. Express* 19:22029–106
3. Jain PK, Lee KS, El-Sayed IH, El-Sayed MA. 2006. Calculated absorption and scattering properties of gold nanoparticles of different size, shape, and composition: applications in biological imaging and biomedicine. *J. Phys. Chem. B* 110:7238–48
4. Maier SA, Atwater HA. 2005. Plasmonics: localization and guiding of electromagnetic energy in metal/dielectric structures. *J. Appl. Phys.* 98:011101
5. Schuller JA, Barnard ES, Cai WS, Jun YC, White JS, Brongersma ML. 2010. Plasmonics for extreme light concentration and manipulation. *Nat. Mater.* 9:193–204
6. Prodan E, Radloff C, Halas NJ, Nordlander P. 2003. A hybridization model for the plasmon response of complex nanostructures. *Science* 302:419–22
7. Halas NJ, Lal S, Chang WS, Link S, Nordlander P. 2011. Plasmons in strongly coupled metallic nanostructures. *Chem. Rev.* 111:3913–61
8. Hoflich K, Yang RB, Berger A, Leuchs G, Christiansen S. 2011. The direct writing of plasmonic gold nanostructures by electron-beam-induced deposition. *Adv. Mater.* 23:2657–61
9. Huang JS, Callegari V, Geisler P, Bruning C, Kern J, et al. 2010. Atomically flat single-crystalline gold nanostructures for plasmonic nanocircuitry. *Nat. Commun.* 1:150
10. Gansel JK, Thiel M, Rill MS, Decker M, Bade K, et al. 2009. Gold helix photonic metamaterial as broadband circular polarizer. *Science* 325:1513–15
11. Jones MR, Osberg KD, Macfarlane RJ, Langille MR, Mirkin CA. 2011. Templated techniques for the synthesis and assembly of plasmonic nanostructures. *Chem. Rev.* 111:3736–827
12. Wang H, Brandl DW, Nordlander P, Halas NJ. 2007. Plasmonic nanostructures: artificial molecules. *Acc. Chem. Res.* 40:53–62
13. Meierhenrich UJ. 2013. Amino acids and the asymmetry of life. *Eur. Rev.* 21:190–99
14. Berova N, Nakanishi K, Woody R. 2000. *Circular Dichroism: Principles and Applications*. New York/Chichester: Wiley-VCH. 877 pp.
15. Barron LD. 2004. *Molecular Light Scattering and Optical Activity*. Cambridge, UK: Cambridge Univ. Press. 443 pp.
16. Rodger A, Nordén B. 1997. *Circular Dichroism and Linear Dichroism*. Oxford, UK: Oxford Univ. Press. 150 pp.

17. Menzel C, Helgert C, Rockstuhl C, Kley EB, Tunnermann A, et al. 2010. Asymmetric transmission of linearly polarized light at optical metamaterials. *Phys. Rev. Lett.* 104:253902
18. Zhang S, Zhou JF, Park YS, Rho J, Singh R, et al. 2012. Photoinduced handedness switching in terahertz chiral metamolecules. *Nat. Commun.* 3:942
19. Valev VK, Baumberg JJ, Sibilia C, Verbiest T. 2013. Chirality and chiroptical effects in plasmonic nanostructures: fundamentals, recent progress, and outlook. *Adv. Mater.* 25:2517–34
20. Schaferling M, Dregely D, Hentschel M, Giessen H. 2012. Tailoring enhanced optical chirality: design principles for chiral plasmonic nanostructures. *Phys. Rev. X* 2:031010
21. Zhao Y, Saleh AAE, Dionne JA. 2016. Enantioselective optical trapping of chiral nanoparticles with plasmonic tweezers. *ACS Photonics* 3:304–9
22. Fasman GD. 1996. *Circular Dichroism and the Conformational Analysis of Biomolecules*. New York: Plenum. 738 pp.
23. Nesterov ML, Yin XH, Schaferling M, Giessen H, Weiss T. 2016. The role of plasmon-generated near fields for enhanced circular dichroism spectroscopy. *ACS Photonics* 3:578–83
24. Chulhai DV, Jensen L. 2015. Plasmonic circular dichroism of 310- and α-helix using a discrete interaction model/quantum mechanics method. *J. Phys. Chem. A* 119:5218–23
25. Hendry E, Carpy T, Johnston J, Popland M, Mikhaylovskiy RV, et al. 2010. Ultrasensitive detection and characterization of biomolecules using superchiral fields. *Nat. Nanotechnol.* 5:783–87
26. Ben-Moshe A, Maoz B, Govorov AO, Markovich G. 2013. Chirality and chiroptical effects in inorganic nanocrystal systems with plasmon and exciton resonances. *Chem. Soc. Rev.* 42:7028–41
27. Ma W, Kuang H, Xu LG, Ding L, Xu CL, et al. 2013. Attomolar DNA detection with chiral nanorod assemblies. *Nat. Commun.* 4:2689
28. Wu XL, Xu LG, Liu LQ, Ma W, Yin HH, et al. 2013. Unexpected chirality of nanoparticle dimers and ultrasensitive chiroplasmonic bioanalysis. *J. Am. Chem. Soc.* 135:18629–36
29. Wang RY, Wang P, Liu YN, Zhao WJ, Zhai DW, et al. 2014. Experimental observation of giant chiroptical amplification of small chiral molecules by gold nanosphere clusters. *J. Phys. Chem. C* 118:9690–95
30. Tullius R, Karimullah AS, Rodier M, Fitzpatrick B, Gadegaard N, et al. 2015. "Superchiral" spectroscopy: detection of protein higher order hierarchical structure with chiral plasmonic nanostructures. *J. Am. Chem. Soc.* 137:8380–83
31. Zhao Y, Askarpour AN, Sun LY, Shi JW, Li XQ, Alu A. 2017. Chirality detection of enantiomers using twisted optical metamaterials. *Nat. Commun.* 8:14180
32. Govorov AO, Fan ZY, Hernandez P, Slocik JM, Naik RR. 2010. Theory of circular dichroism of nanomaterials comprising chiral molecules and nanocrystals: plasmon enhancement, dipole interactions, and dielectric effects. *Nano Lett.* 10:1374–82
33. Govorov AO. 2011. Plasmon-induced circular dichroism of a chiral molecule in the vicinity of metal nanocrystals: application to various geometries. *J. Phys. Chem. C* 115:7914–23
34. Govorov AO, Fan ZY. 2012. Theory of chiral plasmonic nanostructures comprising metal nanocrystals and chiral molecular media. *ChemPhysChem* 13:2551–60
35. Deleted in proof
36. Abdulrahman NA, Fan Z, Tonooka T, Kelly SM, Gadegaard N, et al. 2012. Induced chirality through electromagnetic coupling between chiral molecular layers and plasmonic nanostructures. *Nano Lett.* 12:977–83
37. Schaaff TG, Whetten RL. 2000. Giant gold—glutathione cluster compounds: intense optical activity in metal-based transitions. *J. Phys. Chem. B* 104:2630–41
38. Behar-Levy H, Neumann O, Naaman R, Avnir D. 2007. Chirality induction in bulk gold and silver. *Adv. Mater.* 19:1207–11
39. McPeak KM, van Engers CD, Bianchi S, Rossinelli A, Poulikakos LV, et al. 2015. Ultraviolet plasmonic chirality from colloidal aluminum nanoparticles exhibiting charge-selective protein detection. *Adv. Mater.* 27:6244–50
40. Carmeli I, Lieberman I, Kraversky L, Fan Z, Govorov AO, et al. 2010. Broad band enhancement of light absorption in photosystem I by metal nanoparticle antennas. *Nano Lett.* 10:2069–74

41. Fan ZY, Govorov AO. 2012. Chiral nanocrystals: plasmonic spectra and circular dichroism. *Nano Lett.* 12:3283–89
42. Yan J, Hou S, Ji Y, Wu X. 2016. Heat-enhanced symmetry breaking in dynamic gold nanorod oligomers: the importance of interface control. *Nanoscale* 8:10030–34
43. Levi-Belenkova T, Govorov AO, Markovich G. 2016. Orientation-sensitive peptide-induced plasmonic circular dichroism in silver nanocubes. *J. Phys. Chem. C* 120:12751–56
44. Li T, Park HG, Lee H-S, Choi S-H. 2004. Circular dichroism study of chiral biomolecules conjugated with silver nanoparticles. *Nanotechnology* 15:S660
45. George J, Thomas KG. 2010. Surface plasmon coupled circular dichroism of Au nanoparticles on peptide nanotubes. *J. Am. Chem. Soc.* 132:2502–3
46. Slocik JM, Govorov AO, Naik RR. 2011. Plasmonic circular dichroism of peptide-functionalized gold nanoparticles. *Nano Lett.* 11:701–5
47. Lieberman I, Shemer G, Fried T, Kosower EM, Markovich G. 2008. Plasmon-resonance-enhanced absorption and circular dichroism. *Angew. Chem. Int. Ed.* 47:4855–57
48. McPeak KM, van Engers CD, Bianchi S, Rossinelli A, Poulikakos LV, et al. 2015. Ultraviolet plasmonic chirality from colloidal aluminum nanoparticles exhibiting charge-selective protein detection. *Adv. Mater.* 27:6244–50
49. Shemer G, Krichevski O, Markovich G, Molotsky T, Lubitz I, Kotlyar AB. 2006. Chirality of silver nanoparticles synthesized on DNA. *J. Am. Chem. Soc.* 128:11006–7
50. Maoz BM, van der Weegen R, Fan Z, Govorov AO, Ellestad G, et al. 2012. Plasmonic chiroptical response of silver nanoparticles interacting with chiral supramolecular assemblies. *J. Am. Chem. Soc.* 134:17807–13
51. Maoz BM, Chaikin Y, Tesler AB, Bar Elli O, Fan Z, et al. 2013. Amplification of chiroptical activity of chiral biomolecules by surface plasmons. *Nano Lett.* 13:1203–9
52. di Gregorio MC, Ben Moshe A, Tirosh E, Galantini L, Markovich G. 2015. Chiroptical study of plasmon–molecule interaction: the case of interaction of glutathione with silver nanocubes. *J. Phys. Chem. C* 119:17111–16
53. Lu F, Tian Y, Liu M, Su D, Zhang H, et al. 2013. Discrete nanocubes as plasmonic reporters of molecular chirality. *Nano Lett.* 13:3145–51
54. Hou S, Yan J, Hu Z, Wu X. 2016. Enhancing the plasmonic circular dichroism by entrapping chiral molecules at the core–shell interface of rod-shaped Au@Ag nanocrystals. *Chem. Commun.* 52:2059–62
55. Lan X, Wang Q. 2016. Optically active AuNR@Ag core-shell nanoparticles and hierarchical assembly via DNA-mediated surface chemistry. *ACS Appl. Mater. Interfaces* 8:34598–602
56. Wu X, Xu L, Ma W, Liu L, Kuang H, et al. 2015. Gold core-DNA-silver shell nanoparticles with intense plasmonic chiroptical activities. *Adv. Funct. Mater.* 25:850–54
57. Hao C, Xu L, Ma W, Wu X, Wang L, et al. 2015. Unusual circularly polarized photocatalytic activity in nanogapped gold–silver chiroplasmonic nanostructures. *Adv. Funct. Mater.* 25:5816–22
58. Graf P, Mantion A, Haase A, Thünemann AF, Mašić A, et al. 2011. Silicification of peptide-coated silver nanoparticles—a biomimetic soft chemistry approach toward chiral hybrid core–shell materials. *ACS Nano* 5:820–33
59. Liu W, Zhu Z, Deng K, Li Z, Zhou Y, et al. 2013. Gold nanorod@chiral mesoporous silica core–shell nanoparticles with unique optical properties. *J. Am. Chem. Soc.* 135:9659–64
60. Wen T, Hou S, Yan J, Zhang H, Liu W, et al. 2014. L-cysteine-induced chiroptical activity in assemblies of gold nanorods and its use in ultrasensitive detection of copper ions. *RSC Adv.* 4:45159–62
61. Han B, Shi L, Gao X, Guo J, Hou K, et al. 2016. Ultra-stable silica-coated chiral Au-nanorod assemblies: core–shell nanostructures with enhanced chiroptical properties. *Nano Res.* 9:451–57
62. Zhu Z, Liu W, Li Z, Han B, Zhou Y, et al. 2012. Manipulation of collective optical activity in one-dimensional plasmonic assembly. *ACS Nano* 6:2326–32
63. Layani ME, Ben Moshe A, Varenik M, Regev O, Zhang H, et al. 2013. Chiroptical activity in silver cholate nanostructures induced by the formation of nanoparticle assemblies. *J. Phys. Chem. C* 117:22240–44

64. Kneer LM, Roller EM, Besteiro LV, Schreiber R, Govorov AO, Liedl T. 2018. Circular dichroism of chiral molecules in DNA-assembled plasmonic hotspots. *ACS Nano* 12:9110–15
65. Wu T, Ren J, Wang R, Zhang X. 2014. Competition of chiroptical effect caused by nanostructure and chiral molecules. *J. Phys. Chem. C* 118:20529–37
66. Mark AG, Gibbs JG, Lee TC, Fischer P. 2013. Hybrid nanocolloids with programmed three-dimensional shape and material composition. *Nat. Mater.* 12:802–7
67. Lee HE, Ahn HY, Mun J, Lee YY, Kim M, et al. 2018. Amino-acid- and peptide-directed synthesis of chiral plasmonic gold nanoparticles. *Nature* 556:360–65
68. Ben-Moshe A, Wolf SG, Bar Sadan M, Houben L, Fan ZY, et al. 2014. Enantioselective control of lattice and shape chirality in inorganic nanostructures using chiral biomolecules. *Nat. Commun.* 5:4302
69. Fan ZY, Govorov AO. 2010. Plasmonic circular dichroism of chiral metal nanoparticle assemblies. *Nano Lett.* 10:2580–87
70. Fan ZY, Govorov AO. 2011. Helical metal nanoparticle assemblies with defects: plasmonic chirality and circular dichroism. *J. Phys. Chem. C* 115:13254–61
71. Kuzyk A, Schreiber R, Fan ZY, Pardatscher G, Roller EM, et al. 2012. DNA-based self-assembly of chiral plasmonic nanostructures with tailored optical response. *Nature* 483:311–14
72. Fan ZY, Zhang H, Govorov AO. 2013. Optical properties of chiral plasmonic tetramers: circular dichroism and multipole effects. *J. Phys. Chem. C* 117:14770–77
73. Ferry VE, Smith JM, Alivisatos AP. 2014. Symmetry breaking in tetrahedral chiral plasmonic nanoparticle assemblies. *ACS Photonics* 1:1189–96
74. Jung SH, Jeon J, Kim H, Jaworski J, Jung JH. 2014. Chiral arrangement of achiral Au nanoparticles by supramolecular assembly of helical nanofiber templates. *J. Am. Chem. Soc.* 136:6446–52
75. Molotsky T, Tamarin T, Moshe AB, Markovich G, Kotlyar AB. 2010. Synthesis of chiral silver clusters on a DNA template. *J. Phys. Chem. C* 114:15951–54
76. Jones MR, Osberg KD, Macfarlane RJ, Langille MR, Mirkin CA. 2011. Templated techniques for the synthesis and assembly of plasmonic nanostructures. *Chem. Rev.* 111:3736–827
77. Puma G. 2013. Ag/AgCl@helical chiral TiO_2 nanofibers as a visible-light driven plasmon photocatalyst. *Chem. Commun.* 49:10367–69
78. Hou S, Zhang H, Yan J, Ji YL, Wen T, et al. 2015. Plasmonic circular dichroism in side-by-side oligomers of gold nanorods: the influence of chiral molecule location and interparticle distance. *Phys. Chem. Chem. Phys.* 17:8187–93
79. Han B, Shi L, Gao XQ, Guo J, Hou K, et al. 2016. Ultra-stable silica-coated chiral Au-nanorod assemblies: core-shell nanostructures with enhanced chiroptical properties. *Nano Res.* 9:451–57
80. Aggeli A, Nyrkova IA, Bell M, Harding R, Carrick L, et al. 2001. Hierarchical self-assembly of chiral rod-like molecules as a model for peptide β-sheet tapes, ribbons, fibrils, and fibers. *PNAS* 98:11857–62
81. Bellesia G, Shea J-E. 2007. Self-assembly of β-sheet forming peptides into chiral fibrillar aggregates. *J. Chem. Phys.* 126:245104
82. Duan P, Qin L, Zhu X, Liu M. 2011. Hierarchical self-assembly of amphiphilic peptide dendrons: evolution of diverse chiral nanostructures through hydrogel formation over a wide pH range. *Chem. Eur. J.* 17:6389–95
83. Freire F, Seco JM, Quiñoá E, Riguera R. 2012. Nanospheres with tunable size and chirality from helical polymer–metal complexes. *J. Am. Chem. Soc.* 134:19374–83
84. Ye H-M, Wang J-S, Tang S, Xu J, Feng X-Q, et al. 2010. Surface stress effects on the bending direction and twisting chirality of lamellar crystals of chiral polymer. *Macromolecules* 43:5762–70
85. Wei C. 2006. Radius and chirality dependent conformation of polymer molecule at nanotube interface. *Nano Lett.* 6:1627–31
86. Yashima E, Maeda K, Nishimura T. 2004. Detection and amplification of chirality by helical polymers. *Chem. Eur. J.* 10:42–51
87. Heinz H, Farmer BL, Pandey RB, Slocik JM, Patnaik SS, et al. 2009. Nature of molecular interactions of peptides with gold, palladium, and Pd–Au bimetal surfaces in aqueous solution. *J. Am. Chem. Soc.* 131:9704–14

88. Shemetov AA, Nabiev I, Sukhanova A. 2012. Molecular interaction of proteins and peptides with nanoparticles. *ACS Nano* 6:4585–602
89. Majzik A, Fülöp L, Csapó E, Bogár F, Martinek T, et al. 2010. Functionalization of gold nanoparticles with amino acid, β-amyloid peptides and fragment. *Colloids Surf. B* 81:235–41
90. Chen C-L, Zhang P, Rosi NL. 2008. A new peptide-based method for the design and synthesis of nanoparticle superstructures: construction of highly ordered gold nanoparticle double helices. *J. Am. Chem. Soc.* 130:13555–57
91. Chen C-L, Rosi NL. 2010. Preparation of unique 1-D nanoparticle superstructures and tailoring their structural features. *J. Am. Chem. Soc.* 132:6902–3
92. Song C, Blaber MG, Zhao G, Zhang P, Fry HC, et al. 2013. Tailorable plasmonic circular dichroism properties of helical nanoparticle superstructures. *Nano Lett.* 13:3256–61
93. Zhang C, Song C, Fry HC, Rosi NL. 2014. Peptide conjugates for directing the morphology and assembly of 1D nanoparticle superstructures. *Chem. Eur. J.* 20:941–45
94. Merg AD, Slocik J, Blaber MG, Schatz GC, Naik R, Rosi NL. 2015. Adjusting the metrics of 1-D helical gold nanoparticle superstructures using multivalent peptide conjugates. *Langmuir* 31:9492–501
95. Merg AD, Boatz JC, Mandal A, Zhao G, Mokashi-Punekar S, et al. 2016. Peptide-directed assembly of single-helical gold nanoparticle superstructures exhibiting intense chiroptical activity. *J. Am. Chem. Soc.* 138:13655–63
96. Zhu L, Li X, Wu S, Nguyen KT, Yan H, et al. 2013. Chirality control for in situ preparation of gold nanoparticle superstructures directed by a coordinatable organogelator. *J. Am. Chem. Soc.* 135:9174–80
97. Li Y, Liu M. 2008. Fabrication of chiral silver nanoparticles and chiral nanoparticulate film via organogel. *Chem. Commun.* 43:5571–73
98. Che S, Liu Z, Ohsuna T, Sakamoto K, Terasaki O, Tatsumi T. 2004. Synthesis and characterization of chiral mesoporous silica. *Nature* 429:281–84
99. Qiu H, Che S. 2011. Chiral mesoporous silica: chiral construction and imprinting via cooperative self-assembly of amphiphiles and silica precursors. *Chem. Soc. Rev.* 40:1259–68
100. Ma L, Huang Z, Duan Y, Shen X, Che S. 2015. Optically active chiral Ag nanowires. *Sci. China Mater.* 58:441–46
101. Xie JJ, Duan YY, Che SA. 2012. Chirality of metal nanoparticles in chiral mesoporous silica. *Adv. Funct. Mater.* 22:3784–92
102. Xie J, Che S. 2012. Chirality of anisotropic metal nanowires with a distinct multihelix. *Chem. Eur. J.* 18:15954–59
103. Wang L, Dong H, Li Y, Xue C, Sun L-D, et al. 2014. Reversible near-infrared light directed reflection in a self-organized helical superstructure loaded with upconversion nanoparticles. *J. Am. Chem. Soc.* 136:4480–83
104. Wang L, Dong H, Li Y, Liu R, Wang YF, et al. 2015. Luminescence-driven reversible handedness inversion of self-organized helical superstructures enabled by a novel near-infrared light nanotransducer. *Adv. Mater.* 27:2065–69
105. Zheng Z-G, Li Y, Bisoyi HK, Wang L, Bunning TJ, Li Q. 2016. Three-dimensional control of the helical axis of a chiral nematic liquid crystal by light. *Nature* 531:352–56
106. Bisoyi HK, Li Q. 2016. Light-directed dynamic chirality inversion in functional self-organized helical superstructures. *Angew. Chem. Int. Ed.* 55:2994–3010
107. Qu D, Zhang J, Chu G, Jiang H, Wu C, Xu Y. 2016. Chiral fluorescent films of gold nanoclusters and photonic cellulose with modulated fluorescence emission. *J. Mater. Chem. C* 4:1764–68
108. Thérien-Aubin H, Lukach A, Pitch N, Kumacheva E. 2015. Coassembly of nanorods and nanospheres in suspensions and in stratified films. *Angew. Chem.* 127:5710–14
109. Lukach A, Thérien-Aubin H, Querejeta-Fernández A, Pitch N, Chauve G, et al. 2015. Coassembly of gold nanoparticles and cellulose nanocrystals in composite films. *Langmuir* 31:5033–41
110. Vollick B, Kuo P-Y, Thérien-Aubin H, Yan N, Kumacheva E. 2016. Composite cholesteric nanocellulose films with enhanced mechanical properties. *Chem. Mater.* 29:789–95

111. Chu G, Wang X, Yin H, Shi Y, Jiang H, et al. 2015. Free-standing optically switchable chiral plasmonic photonic crystal based on self-assembled cellulose nanorods and gold nanoparticles. *ACS Appl. Mater. Interfaces* 7:21797–806
112. Chu G, Wang X, Chen T, Gao J, Gai F, et al. 2015. Optically tunable chiral plasmonic guest–host cellulose films weaved with long-range ordered silver nanowires. *ACS Appl. Mater. Interfaces* 7:11863–70
113. Querejeta-Fernández A, Chauve G, Methot M, Bouchard J, Kumacheva E. 2014. Chiral plasmonic films formed by gold nanorods and cellulose nanocrystals. *J. Am. Chem. Soc.* 136:4788–93
114. Querejeta-Fernández A, Kopera B, Prado KS, Klinkova A, Methot M, et al. 2015. Circular dichroism of chiral nematic films of cellulose nanocrystals loaded with plasmonic nanoparticles. *ACS Nano* 9:10377–85
115. Wang R-Y, Wang H, Wu X, Ji Y, Wang P, et al. 2011. Chiral assembly of gold nanorods with collective plasmonic circular dichroism response. *Soft Matter* 7:8370–75
116. Guerrero-Martínez A, Auguié B, Alonso-Gómez JL, Džolić Z, Gómez-Graña S, et al. 2011. Intense optical activity from three-dimensional chiral ordering of plasmonic nanoantennas. *Angew. Chem. Int. Ed.* 50:5499–503
117. Kim Y, Yeom B, Arteaga O, Yoo SJ, Lee S-G, et al. 2016. Reconfigurable chiroptical nanocomposites with chirality transfer from the macro- to the nanoscale. *Nat. Mater.* 15:461–68
118. Yan WJ, Xu LG, Xu CL, Ma W, Kuang H, et al. 2012. Self-assembly of chiral nanoparticle pyramids with strong R/S optical activity. *J. Am. Chem. Soc.* 134:15114–21
119. Li ZT, Zhu ZN, Liu WJ, Zhou YL, Han B, et al. 2012. Reversible plasmonic circular dichroism of Au nanorod and DNA assemblies. *J. Am. Chem. Soc.* 134:3322–25
120. Wu XL, Xu LG, Ma W, Liu LQ, Kuang H, et al. 2016. Propeller-like nanorod-upconversion nanoparticle assemblies with intense chiroptical activity and luminescence enhancement in aqueous phase. *Adv. Mater.* 28:5907–15
121. Rothemund PW. 2006. Folding DNA to create nanoscale shapes and patterns. *Nature* 440:297–302
122. Mastroianni AJ, Claridge SA, Alivisatos AP. 2009. Pyramidal and chiral groupings of gold nanocrystals assembled using DNA scaffolds. *J. Am. Chem. Soc.* 131:8455–59
123. Alivisatos AP, Johnsson KP, Peng XG, Wilson TE, Loweth CJ, et al. 1996. Organization of "nanocrystal molecules" using DNA. *Nature* 382:609–11
124. Yan WJ, Xu LG, Ma W, Liu LQ, Wang LB, et al. 2014. Pyramidal sensor platform with reversible chiroptical signals for DNA detection. *Small* 10:4293–97
125. Li S, Xu LG, Ma W, Wu XL, Sun MZ, et al. 2016. Dual-mode ultrasensitive quantification of microRNA in living cells by chiroplasmonic nanopyramids self-assembled from gold and upconversion nanoparticles. *J. Am. Chem. Soc.* 138:306–12
126. Zhao Y, Xu LG, Ma W, Wang LB, Kuang H, et al. 2014. Shell-engineered chiroplasmonic assemblies of nanoparticles for zeptomolar DNA detection. *Nano Lett.* 14:3908–13
127. Ma W, Kuang H, Wang LB, Xu LG, Chang WS, et al. 2013. Chiral plasmonics of self-assembled nanorod dimers. *Sci. Rep.* 3:1934
128. Chen W, Bian A, Agarwal A, Liu LQ, Shen HB, et al. 2009. Nanoparticle superstructures made by polymerase chain reaction: collective interactions of nanoparticles and a new principle for chiral materials. *Nano Lett.* 9:2153–59
129. Pal S, Deng Z, Wang H, Zou S, Liu Y, Yan H. 2011. DNA directed self-assembly of anisotropic plasmonic nanostructures. *J. Am. Chem. Soc.* 133:17606–9
130. Shen X, Song C, Wang J, Shi D, Wang Z, et al. 2011. Rolling up gold nanoparticle-dressed DNA origami into three-dimensional plasmonic chiral nanostructures. *J. Am. Chem. Soc.* 134:146–49
131. Shen XB, Asenjo-Garcia A, Liu Q, Jiang Q, García de Abajo FJ, et al. 2013. Three-dimensional plasmonic chiral tetramers assembled by DNA origami. *Nano Lett.* 13:2128–33
132. Tian Y, Wang T, Liu W, Xin HL, Li H, et al. 2015. Prescribed nanoparticle cluster architectures and low-dimensional arrays built using octahedral DNA origami frames. *Nat. Nanotechnol.* 10:637–44
133. Urban MJ, Dutta PK, Wang PF, Duan XY, Shen XB, et al. 2016. Plasmonic toroidal metamolecules assembled by DNA origami. *J. Am. Chem. Soc.* 138:5495–98

134. Dai GL, Lu XX, Chen Z, Meng C, Ni WH, Wang QB. 2014. DNA origami-directed, discrete three-dimensional plasmonic tetrahedron nanoarchitectures with tailored optical chirality. *ACS Appl. Mater. Interfaces* 6:5388–92
135. Rao C, Wang ZG, Li N, Zhang W, Xu X, Ding B. 2015. Tunable optical activity of plasmonic dimers assembled by DNA origami. *Nanoscale* 7:9147–52
136. Shen CQ, Lan X, Lu XX, Ni WH, Wang QB. 2015. Tuning the structural asymmetries of three-dimensional gold nanorod assemblies. *Chem. Commun.* 51:13627–29
137. Chen Z, Lan X, Chiu YC, Lu XX, Ni WH, et al. 2015. Strong chiroptical activities in gold nanorod dimers assembled using DNA origami templates. *ACS Photonics* 2:392–97
138. Shen XB, Zhan PF, Kuzyk A, Liu Q, Asenjo-Garcia A, et al. 2014. 3D plasmonic chiral colloids. *Nanoscale* 6:2077–81
139. Lan X, Chen Z, Dai G, Lu X, Ni W, Wang Q. 2013. Bifacial DNA origami-directed discrete, three-dimensional, anisotropic plasmonic nanoarchitectures with tailored optical chirality. *J. Am. Chem. Soc.* 135:11441–44
140. Lan X, Lu X, Shen C, Ke Y, Ni W, Wang Q. 2015. Au nanorod helical superstructures with designed chirality. *J. Am. Chem. Soc.* 137:457–62
141. Edwardson TG, Lau KL, Bousmail D, Serpell CJ, Sleiman HF. 2016. Transfer of molecular recognition information from DNA nanostructures to gold nanoparticles. *Nat. Chem.* 8:162–70
142. Zhang Y, Chao J, Liu H, Wang F, Su S, et al. 2016. Transfer of two-dimensional oligonucleotide patterns onto stereocontrolled plasmonic nanostructures through DNA-origami-based nanoimprinting lithography. *Angew. Chem. Int. Ed.* 55:8036–40
143. Gu HZ, Chao J, Xiao SJ, Seeman NC. 2010. A proximity-based programmable DNA nanoscale assembly line. *Nature* 465:202–5
144. Cecconello A, Kahn JS, Lu CH, Khorashad LK, Govorov AO, Willner I. 2016. DNA scaffolds for the dictated assembly of left-/right-handed plasmonic Au NP helices with programmed chiro-optical properties. *J. Am. Chem. Soc.* 138:9895–901
145. Schreiber R, Luong N, Fan ZY, Kuzyk A, Nickels PC, et al. 2013. Chiral plasmonic DNA nanostructures with switchable circular dichroism. *Nat. Commun.* 4:2948
146. Kuzyk A, Schreiber R, Zhang H, Govorov AO, Liedl T, Liu N. 2014. Reconfigurable 3D plasmonic metamolecules. *Nat. Mater.* 13:862–66
147. Kuzyk A, Yang Y, Duan X, Stoll S, Govorov AO, et al. 2016. A light-driven three-dimensional plasmonic nanosystem that translates molecular motion into reversible chiroptical function. *Nat. Commun.* 7:10591
148. Kuzyk A, Urban MJ, Idili A, Ricci F, Liu N. 2017. Selective control of reconfigurable chiral plasmonic metamolecules. *Sci. Adv.* 3:e1602803
149. Zhou C, Duan X, Liu N. 2015. A plasmonic nanorod that walks on DNA origami. *Nat. Commun.* 6:8102
150. Urban MJ, Zhou C, Duan X, Liu N. 2015. Optically resolving the dynamic walking of a plasmonic walker couple. *Nano Lett.* 15:8392–96
151. Zhang H, Govorov AO. 2013. Giant circular dichroism of a molecule in a region of strong plasmon resonances between two neighboring gold nanocrystals. *Phys. Rev. B* 87:075410